Dynamics of CO in Mesoporous Silica Monitored by Time-Resolved Step-Scan and Rapid-Scan FT-IR Spectroscopy

Lars Klembt Andersen and Heinz Frei*

Physical Biosciences Division, Lawrence Berkeley National Laboratory, University of California, Berkeley, California 94720

Received: June 27, 2006; In Final Form: September 11, 2006

Carbon monoxide molecules generated in the channels of mesoporous MCM-41 silica sieve from a precursor (diphenyl cyclopropenone) by photodissociation with a nanosecond laser pulse were monitored by time-resolved Fourier transform infrared (FTIR) spectroscopy using the step-scan and rapid-scan methods. A very broad absorption of CO is observed in the region 2200−2080 cm^{-1} at room temperature that decays in a biphasic mode. Two-thirds of the band intensity decays on the hundreds of microsecond scale (lifetime 344 ± 70 μs). The process represents the escape of the molecules through the mesopores into the surrounding gas phase, and a diffusion constant of 1.5×10^{-9} m^2/s is derived (assuming control by intra-MCM-41 particle diffusion). The broad profile of the absorption is attributed to contact of the random hopping CO with siloxane and silanol groups of the pore surface. Measurements using MCM-41 with the silanols partially capped by trimethyl silyl groups gave further insight into the nature of the IR band profile. These are the first observations on the diffusion behavior of carbon monoxide in a mesoporous material at room temperature. The residual carbon monoxide remains much longer in the pores and features distinct peaks at 2167 and 2105 cm^{-1} characteristic for CO adsorbed on SiOH groups C end on and O end on, respectively. The bands decrease with time constants of 113 ± 3 ms (2167 cm^{-1}) and 155 ± 15 ms (2105 cm^{-1}) suggesting that CO in these sites is additionally trapped by surrounding diphenyl acetylene coproduct and/or precursor molecules.

1. Introduction

A mesoporous silica sieve of type MCM-41 has recently been employed as nanostructured high surface area support of single or binuclear transition metal sites for the photoreduction of CO_2 to CO. The material $ZrCu^{I}$−MCM-41 featuring binuclear Zr^{IV}−O−Cu^{I} centers on the pore surface affords splitting of adsorbed CO_2 to CO by photoexcitation of the metal-to-metal charge-transfer chromophore.[1] For this material, the resulting carbon monoxide is trapped inside the mesopores by coordinating to isolated Cu^{I} centers anchored on the silica surface. On the other hand, when conducting photoreduction of CO_2 gas by H_2O in a framework substituted TiMCM-41 sieve by single photon excitation of the Ti−O ligand-to-metal charge-transfer transition in the UV, gas-phase CO is observed by in-situ FTIR spectroscopy. Steady-state IR monitoring of the photochemical reaction at room-temperature did not reveal any adsorbed CO inside the material.[2] Yet, since the photoactivation of CO_2 takes place at Ti centers inside the pores, the CO product must reside, however brief, in the mesoporous channels before diffusing out of the pores into the gas phase. Clearly, sites with CO affinity present in the pores, as well as the specific pore structure of these silicates may directly affect the diffusion properties of CO. These may in turn affect the performance of these mesoporous silicates in the photocatalytic reduction of CO_2 to CO, for example, by either suppressing or facilitating back reaction. It is thus crucial to understand the diffusion of CO in these materials.

Diffusion of CO in porous solids has thus far been studied in zeolites using the pulsed field gradient (PFG) ^{13}C NMR technique[3−6] or the frequency response technique.[7] A few reports also discuss long-range (intercrystalline) diffusion of CO in packed zeolite crystals.[5,6,8] By contrast to work on these microporous crystalline materials, no measurements have been reported on carbon monoxide diffusion in mesoporous silicas. A number of diffusion studies in MCM-41 have focused on medium size alkanes.[9−11] The residence time of very small gaseous molecules such as CO inside mesoporous particles of typical size (one to a few micrometers) might be too short for monitoring by PFG NMR methods. On the other hand, fast time-resolved step-scan FTIR absorption spectroscopy has recently allowed us to monitor short-lived radicals (formyl, acetyl radical) in zeolites.[12−16] This technique relies on the generation of the species of interest from a photolabile precursor with a nanosecond laser pulse, and the temporal resolution of the step-scan method covers the continuous range from 20 nanoseconds to milliseconds. Slower processes can be monitored by the rapid-scan FTIR method covering the range from 15 milliseconds to seconds. The wide time span of the combined techniques is likely to encompass the time it takes for CO molecules to escape from the mesopores of MCM-41 particles. We thus set out to monitor the diffusion of CO generated inside the mesopores of MCM-41 at room temperature using these techniques. Transient CO was generated by photodissociation of diphenyl cyclopropenone (DPCP) present inside the solvent-free mesopores of MCM-41 using a nanosecond UV laser pulse.[17] The precursor was selected based on the ultrafast dissociation time and a quantum yield close to 1.[17]

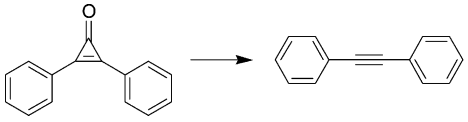

(1)

* To whom correspondence should be addressed. E-mail: hmfrei@lbl.gov.

10.1021/jp0640326 CCC: $33.50
Published on Web 10/18/2006

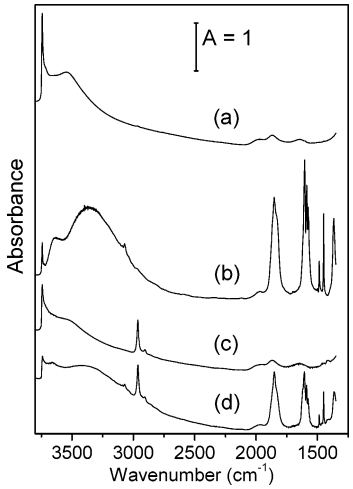

Figure 1. Static FTIR absorption spectra of (a) MCM-41, (b) MCM-41 loaded with diphenyl cyclopropenone (DPCP), (c) Trimethylchlorosilane-treated MCM-41 (TMS-MCM-41), and (d) TMS-MCM-41 loaded with DPCP.

We report here the spectral and temporal evolution of CO as the molecules escape from the pores into the gas phase.

2. Experimental Section

MCM-41 sieve was prepared according to a method described previously.[18] Briefly, 2.2 g of cetyltrimethylammonium bromide (CTAB template, Aldrich) was dissolved in 52 mL of water at 40 °C. Ammonium hydroxide (Aldrich, 26 mL, 30%) was then added under stirring. Addition of 10 mL of tetraethoxysilane (Fluka, puriss.) to the solution was followed by continued stirring for 3 h at 20 °C. The gel was transferred to a Teflon-lined autoclave and held at 110 °C for 48 h. Filtration and washing with distilled H_2O gave the product. Template removal was conducted by heating at 300 °C for 2 h followed by calcination in air at 550 °C for 12 h.

Partial trimethylsilylation of calcined MCM-41 was performed according to the literature.[19] Briefly, calcined MCM-41 was dehydrated at 110 °C under vacuum (10 mTorr) overnight. The temperature was then raised to 260 °C so as to effect partial dehydroxylation of the hydrogen-bonded silanol network, and after 1 h, the sample was exposed to 100 Torr of trimethylchlorosilane (Aldrich, >99%). The gas phase was pumped off, and the silane reintroduced 3 times during the next 4 h. Hereafter, the gas phase was pumped off, and the sample was left to cool slowly under vacuum for 4 h. Trimethylchlorosilane reacts with silanol groups inside (and outside) the mesopores of MCM-41 to form trimethylsilyloxy groups anchored on the silica surface.[19] Figure 1 shows the static FTIR spectra of calcined MCM-41 before (trace a) and after silylation (trace c). The loss in hydrogen bonded (broad 3545 cm^{-1}) and free silanol (3745 cm^{-1}) concomitant with the incorporation of trimethylsilyl groups (2960 cm^{-1}) is evident. From the loss in free silanol, and by comparing the intensity of these bands to those in close to fully silylated MCM-41 (conducted at high temperature, spectra not shown), we estimate that approximately 50% of the silanols were capped by trimethylsilyl groups using the low-temperature silylation scheme described here. The trimethylchlorosilane-treated MCM-41 will be referred to as 'TMS-MCM-41' to distinguish it from the nontreated "plain MCM-41".

Diphenyl cyclopropenone (DPCP, Acros, 98%) was incorporated into calcined MCM-41 and TMS-MCM-41 by stirring the silica powder in a solution of DPCP in CH_2Cl_2/heptane = 1:1 (Aldrich, >99%) for 12 h followed by vacuum filtration. The uptake of 5−10 wt % was derived from the UV−vis spectroscopy of the supernatant and confirmed by FTIR spectroscopy of DPCP in plain MCM-41 (Figure 1, trace b) and DPCP in TMS-MCM-41 (Figure 1, trace d). As-synthesized MCM-41 (CTAB template still present in the mesopores) did not display any uptake of DPCP, which confirms that DPCP was indeed incorporated into the mesopores of calcined plain MCM-41 and TMS-MCM-41.

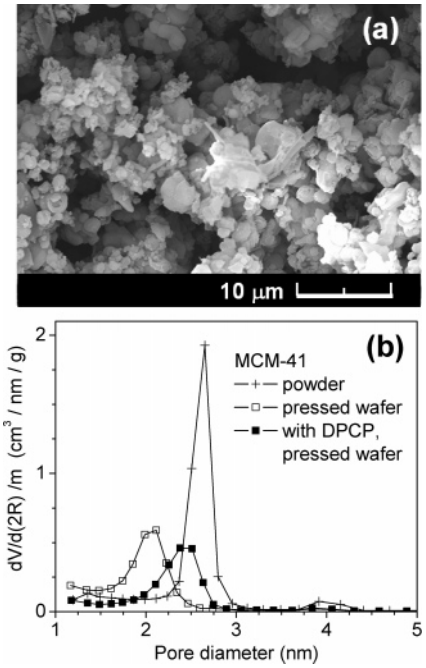

Figure 2. (a) SEM image of MCM-41 powder and (b) pore size distribution (derived from 77 K N_2 isotherms) for MCM-41 as powder, pressed wafer, and loaded with DPCP and pressed into wafer. Ordinate: volume of pores with a given diameter (2R) per gram of MCM-41.

SEM images of gold-coated samples of calcined and TMS-MCM-41 with or without DPCP loading all showed the same grain size, typically 1 μ across, with an abundance of open voids between the particles as can be seen from Figure 2a. Powder X-ray diffraction (XRD) measurements (Siemens model D500 Cu K_α) on all MCM-41 materials showed the same Bragg peaks (4.0 nm long-range order) as reported in the literature for MCM-41.[20] Specifically, no change in position was observed upon trimethylsilylation and loading of DPCP or upon pressing the materials into wafers. Pore size distributions were derived from 77 K N_2 sorption experiments (Quantachrome Autosorb-1 using the Kelvin equation and BJH-method) for all materials (Figure 2b). The mesopores are seen as peaks in the distributions with diameters ranging from 2.0 to 2.65 nm depending on powder or wafer form or whether DPCP is loaded into the pores. For plain MCM-41 powder, a total mesopore volume of 0.60 cm^3/g and surface area of about 900 m^2/g was measured. From the pore diameter, pore volume, and surface area, a geometrical pore wall area of 5500 nm^2 per 1 μ pore length is estimated.

Self-supporting wafers (10 mg, 110 μ thick, 12 mm diameter) of MCM-41 loaded with DPCP were pressed at 1.5 ton (130 MPa) for 5 s and used for the photolysis experiments. No change in the positions of Bragg peaks in the powder XRD spectrum was observed upon pressing except for a loss in intensity of the peaks, as expected from the modest pressure used here.[21]

On the other hand, the loss of peak intensity of the pore size distribution curve signals a reduction of the portion of mesopores, as is typically observed upon pressing of wafers.[21] The mesopore size of the precursor-loaded sieve is reduced by only 2 Å reflecting the influence of the loading on the pore diameter. The wafers were mounted in a miniature IR vacuum cell equipped with CaF_2 windows, and the cell was positioned inside in the spectrometer sample compartment.[22] The wafers were dehydrated by evacuation at room temperature (RT) overnight. Time-resolved photolysis experiments were conducted at 298 K under continuous evacuation, which assured that the CO generated by each laser pulse was removed from the IR cell before the next pulse arrived. The laser was operated at a repetition rate of 1 Hz, and the IR spectra show that CO is removed completely from the IR cell within 700 ms.

Time-resolved FTIR measurements were conducted with a Bruker Model IFS88 spectrometer. A photovoltaic MCT (HgCdTe) detector Kolmar Model KMPV8-1-J2 with an 8 μm band gap was used ($D^* = 1 \times 10^{11}$ cm $Hz^{1/2}$ W^{-1}). The detector has a 37 ns fwhm response to the 5 ns laser pulse. The detector preamplifier has direct current (dc) and alternating current (ac)-outputs, with the ac output having a RC high-pass filter with a 1.42 ms time constant. To maximize the sensitivity for spectroscopy in the desired spectral region, folding limits were chosen at 2393 and 1915 cm^{-1} requiring an IR filter for blocking off probe light outside this range (OCLI Model W04684-4). The photolysis of DPCP was initiated by 355 nm nanosecond pulses of a Quanta Ray Model DCR2A (GCR-3 upgrade). A quartz prism (1 cm edge-to-edge) was used to align the photolysis beam collinearly with the IR probe beam. To prevent photolysis light entering the detector or interferometer compartment, the ports to these compartments were closed off by germanium plates with dielectric coatings that maximized IR transmission ($T = 95\%$, International Scientific). Experiments were conducted on the nano- and microsecond time scale (0 to 1000 μs) by the step-scan method and on the millisecond time scale (20 to 1000 ms) by the rapid-scan method. In both cases, the data acquisition of the spectrometer was triggered by the photolysis laser pulse using an EG&G Si photodiode, model SGD-444.

Step-scan experiments were conducted as described in the literature.[12−14] Briefly, the ac and dc-coupled interferometric detector signals were simultaneously acquired by a 40 MHz 12 bit digitizer (model PAD 1232). The time resolution of the digitizer was set to 1 μs, and data were recorded from 0 to 530 μs in most experiments (with the 1.42 ms decay constant of the ac output significantly influencing the amplitude of the spectra at times beyond 500 μs). Prior to digitization, the ac-coupled signal was amplified using a CAL-AV Laboratories model 7930 500 MHz amplifier, while the dc-coupled signal was attenuated and the offset adjusted to zero (LeCroy model 6103 programmable amplifier). The signal adjustments ensured use of the full dynamic range (±1 V) of the digitizer. Transient absorbance spectra were calculated as

$$\Delta A = \log \frac{S}{S + \Delta S/\gamma} \qquad (2)$$

(S, static single beam spectrum = FT of dc-coupled interferogram; ΔS, laser-induced spectral change = FT of ac-coupled interferogram; $\gamma = 20$, amplification ratio ac/dc). Spectra were recorded with 8 cm^{-1} resolution requiring 120 single-sided interferogram points (mirror positions). At each mirror position, three laser-induced decays were averaged. In these experiments, the laser energy arriving at the sample was between 2.8 and 5.6 mJ/pulse for an 8 mm laser beam diameter. Depending on the energy, 15 to 25% of the initial amount of DPCP was photolyzed during an experiment (360 laser pulses) as monitored by the decrease of the DPCP IR band at 1850 cm^{-1}. We have shown previously that reactant depletion of this magnitude does not result in measurable distortion of the transient spectra.[15] Data were averaged in 30 μs intervals to yield spectra reported by the midpoint of the interval. The spectra were corrected for the slightly curved baseline found in most step-scan traces.

Rapid-scan experiments were conducted by a modified version of procedures described in detail previously.[12] Briefly, the mirror velocity was 160 kHz, and the spectral resolution was 8 cm^{-1}. The protocol for obtaining the transient spectra consisted of the recording of 99 interferograms (double-sided/forward−backward) following the arrival of the laser pulse, which was triggered by a forward motion of the interferometer mirror. These interferograms thus represent a time sequence after the laser pulse. The first 2 interferograms were further separated into the forward and the backward motion interferograms for increased time resolution. Subsequent interferograms were averaged to obtain a total of 9 interferograms with midpoints located at times 21, 57, 103, 139, 202, 284, 366, 530, and 694 ms after the laser pulses. The first 4 of these interferograms (either forward or backward) were recorded over 26 ms, and the subsequent 5 interferograms (forward and backward) were recorded over 62 ms. Recording of the first interferogram started 8 ms after the laser pulses. The interferograms were Fourier transformed into the corresponding 9 single beam spectra. A total of 50 such sets of single beam spectra generated by 50 laser pulses were stored as the result of one experiment. Final transient absorbance spectra for a given time delay were obtained by calculating the ratio of each of the 50 corresponding stored single beam spectra against the single beam spectrum taken just before the pulse (i.e., single beam spectrum no. 9 from the previous sequence). The 50 absorbance spectra were then averaged to yield the absorbance time slice for a given time delay. The results of typically 10 such experiments were averaged for further S/N improvement. In these experiments, the laser energy arriving at the sample was 7.3 mJ/pulse for 8 mm laser beam diameter. Seven percent of the initial amount of DPCP was photolyzed during an experiment. The last spectrum (694 ms) showed that the CO signal had completely vanished. All spectra shown are subtractions using the 694 ms slice as the baseline.

3. Results

A. CO in Plain MCM-41. The transient absorption spectra recorded upon photolysis of DPCP in plain MCM-41 are shown in Figure 3. The initial trace at 15 μs shows a broad (88 cm^{-1} fwhm (full width at half-maximum)) feature centered at 2130 cm^{-1} (Figure 3a). The band decays on the hundreds of microsecond time scale, with two peaks emerging at 2167 and 2105 cm^{-1} after a few hundred microseconds. These two residual bands decay much more slowly on the time scale of hundreds of milliseconds (Figure 3b). We assign all spectra to CO residing inside the pores of MCM-41 on the basis of the following four observations: (1) The bands are located in the same spectral region 2000−2300 cm^{-1} as previously reported for CO adsorbed inside micro- and mesoporous silicates using cryogenic low-temperature techniques and FTIR.[23−30] (2) The band observed at 15 μs is present already in the first recorded time slice (1 μs after the laser pulse, not shown), a time far too short for escape from the mesopores. The fast formation of CO is in accordance with the instant photodissociation (2 ps) of

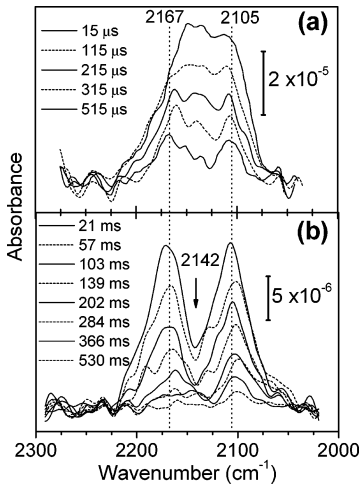

Figure 3. Time-resolved FTIR absorption spectra of CO formed inside MCM-41 recorded upon laser-induced photolysis of DPCP: (a) step-scan FTIR spectra (average of 21 experiments) and (b) rapid-scan FTIR spectra (average of 12 experiments). The rapid-scan spectra were normalized so that (a) and (b) correspond to the same amount of DPCP depleted (and CO produced) per laser pulse. Note that the absorbance scale of the millisecond spectra is enlarged.

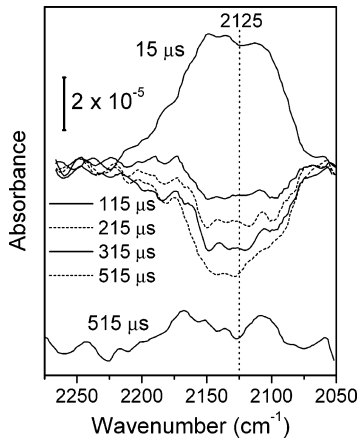

Figure 4. Step-scan FTIR absorption spectra of CO formed inside MCM-41 (same as in Figure 3a). Spectrum 15 μs after the laser pulse, and difference spectra at subsequent times (compared to spectrum at 15 μs), and spectrum 515 μs after the laser pulse are shown.

DPCP to CO and diphenyl acetylene reported in the literature.[17] (3) While the slowly decaying absorptions at 2167 and 2105 cm^{-1} are in the vicinity of the P and R branch of a gaseous CO measured at low spectral resolution (R branch maximum at 2172 cm^{-1}; P branch maximum at 2115 cm^{-1}), there is a clear mismatch that is readily seen when comparing spectra of Figure 3b with a gas-phase CO spectrum. In fact, when the IR cell was not evacuated during the experiment, we observed that the spectra of Figure 3b transformed into a CO gas-phase spectrum on the time scale of 1 s.

To allow further analysis of the initial rapid depletion of CO on the microsecond time scale, the depletion profile was computed and is displayed in Figure 4. The negative traces are the differences between the spectra recorded at 115, 215, 315, and 515 μs and the initial 15 μs trace. The bleach is centered at 2125 cm^{-1} and has a nearly constant fwhm of about 75 cm^{-1} and a weak tail on the high-frequency side. Furthermore, comparison of the intensity of the 515 μs trace (taking into account the correction for the RC constant of the ac coupler) and the 21 ms trace of Figure 3 show that there is no significant change of intensity in the time interval between 500 μs and

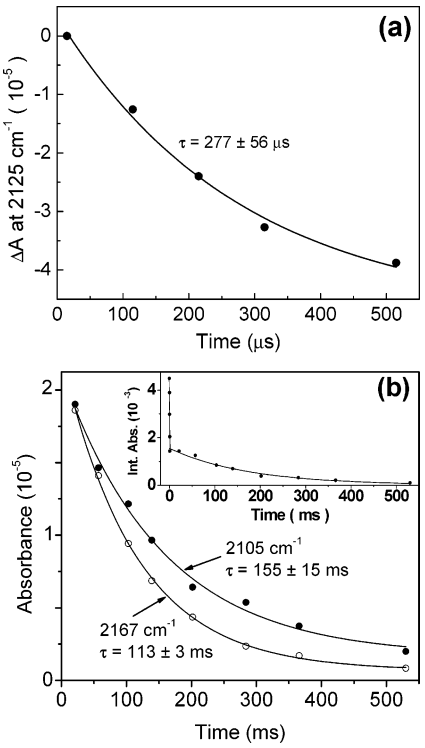

Figure 5. (a) Single-exponential fit of the absorbance difference at 2125 cm^{-1} (Figure 4) yields a decay time of 277 $\pm$ 56 μs. Correcting for the 1420 μs RC high-pass filter of the detector yields 344 $\pm$ 70 μs. (b) Single-exponential fit of the absorbance decay at 2105 and 2167 cm^{-1} (Figure 3b) yields decay times of 155 $\pm$ 15 ms and 113 $\pm$ 3 ms, respectively. The insert shows the decay of the full CO profile (integrated from 2220 to 2060 cm^{-1}) in both the rapid-scan data and the step-scan data (corrected for the RC high-pass filter of the detector). Ordinate unit of insert: 10^{-3} cm^{-1}.

21 ms. Therefore, CO decays in a distinct biphasic mode with the process on the microsecond time scale well separated from the much slower decay on the millisecond scale. This warrants separate kinetic fits for the two processes. Figure 5 shows a single-exponential fit of the absorbance at 2125 cm^{-1} which yields a decay time of t_e = 277 $\pm$ 56 μs (t_e = 344 $\pm$ 70 μs after correction for the RC constant of the ac coupler). Kinetic analysis of the much longer lived 2167 and 2105 cm^{-1} band yields decay times of 113 $\pm$ 3 and 155 $\pm$ 15 ms, respectively (Figure 5b). The different decay times indicate that the bands are associated with two distinctively different CO species. The time evolution of the integrated CO absorption spectrum (2220−2060 cm^{-1}) is shown in the insert in Figure 5b. The biphasic release of CO from the mesopores is clearly seen here.

Static difference spectra before and after photolysis show depletion of the DPCP along with growth of bands at 1444, 1500, and 1595 cm^{-1} and several very weak bands between 3030 and 3100 cm^{-1}. These bands are in excellent agreement with the IR spectrum of the expected photolysis coproduct diphenyl acetylene.[31] Other IR peaks of diphenyl acetylene overlap with DPCP absorptions.

B. CO in Trimethyl Silylated MCM-41. The transient absorption spectra of CO in partial trimethyl silylated MCM-41 are shown in Figure 6. There are clearly similarities between these spectra and those of CO in plain MCM-41: A rapid initial decay within 500 μs of the central portion of the profile is followed by a slow decay of two peaks with maxima at 2106 and 2175 cm^{-1} on the time scale of a few hundred milliseconds. However, there are several notable differences between the two materials. The decay on the microsecond time scale, shown in

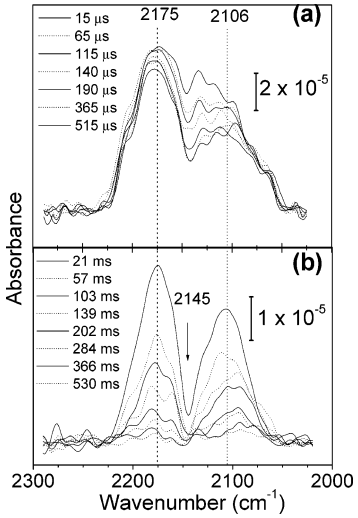

Figure 6. Time-resolved FTIR absorption spectra of CO formed inside trimethylchlorosilane-treated MCM-41 (TMS-MCM-41) recorded upon laser-induced photolysis of DPCP: (a) step-scan FTIR spectra (average of 27 experiments) and (b) rapid-scan FTIR spectra (average of 9 experiments). The rapid-scan spectra were normalized so that (a) and (b) correspond to the same amount of DPCP depleted (and CO produced) per laser pulse. Note that the absorbance scale of the millisecond spectra is enlarged.

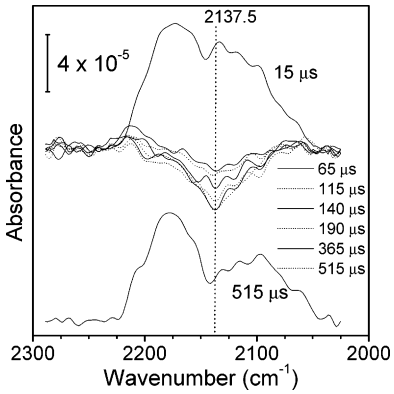

Figure 7. Step-scan FTIR absorption spectra of CO formed inside TMS-MCM-41 (same as in Figure 6a). Spectrum 15 μs after the laser pulse, and difference spectra at subsequent times (compared to spectrum at 15 μs), and spectrum 515 μs after the laser pulse are shown.

Figure 7 as difference spectra with respect to the 15 μs trace, shows a relatively sharp spectrum centered at 2137.5 cm^{-1} (fwhm 47 cm^{-1}) compared to the much broader and flatter depletion profile in plain MCM-41 (Figure 4). Furthermore, in contrast to CO in plain MCM-41, the spectra of CO in TMS-MCM-41 at 515 μs and 21 ms have substantially different intensities; the integrated intensity (normalized to the value at 15 μs) decreases from 78% at 515 μs to 37% at 21 ms, while no significant decrease of the CO band over the same time interval was observed in the case of plain MCM-41. Since the time window between 500 μs and 21 ms was not accessible for reliable intensity measurements with our currently available IR detectors, no quantitative kinetic data for this interval are available. Nevertheless, we find that it takes approximately 20 ms for 60% of the CO to leave TMS-MCM-41, while the same 60% loss of CO takes only 500 μs in plain MCM-41. This is a significant difference in the behavior of CO in the two materials.

While the spectra at 515 μs and on the millisecond time scale feature two main absorption peaks in both TMS treated and plain MCM-41, the band positions and relative intensities in the two hosts are not identical. In TMS-MCM-41, the high-

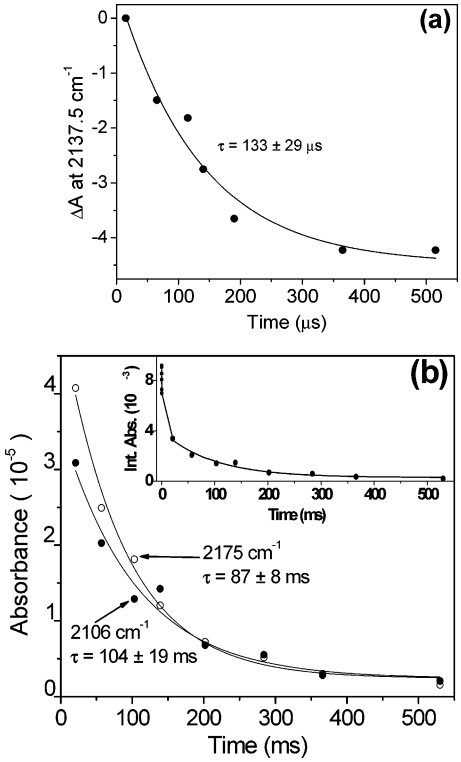

Figure 8. (a) Single-exponential fit of the absorbance difference at 2137.5 cm^{-1} (Figure 7) yields a decay time of 133 $\pm$ 29 μs. Correcting for the 1420 μs RC high-pass filter of the detector yields 147 $\pm$ 29 μs, ordinate unit 10^{-5}. (b) Single-exponential fit of the absorbance decay at 2106 and 2175 cm^{-1} (Figure 6b) yields decay times of 104 $\pm$ 19 ms and 87 $\pm$ 8 ms, respectively. The insert shows the decay of the full CO profile (integrated from 2230 to 2055 cm^{-1}) in both the rapid-scan data and the step-scan data (corrected for the RC high-pass filter of the detector). Ordinate unit of insert: 10^{-3} cm^{-1}.

frequency band is blue shifted by 8 cm^{-1} relative to plain MCM-41 and the 2106 cm^{-1} band is less intense. The change in relative intensity of the 2175 (2167) and the 2106 (2105) cm^{-1} peaks indicates that the high- and low-frequency bands represent two different species of CO inside MCM-41. The absence of data points in the early millisecond regime prevents us from exactly determining the kinetics in this time interval. The discussion of the temporal behavior of CO in the methylated material will thus be based on separate single-exponential fits for the decay on the microsecond (Figure 8a) and long millisecond time scale (Figure 8b). The initial decay constant for the 2137.5 cm^{-1} peak corresponds to a lifetime of t_e = 147 $\pm$ 29 μs (corrected for the RC constant of the ac coupler), while the corresponding rates for the slowly decaying 2175 and 2106 cm^{-1} bands are 87 $\pm$ 8 ms and 104 $\pm$ 19 ms, respectively. The overall decay in the integrated CO band (2230−2055 cm^{-1}) is shown in the insert in Figure 8b.

4. Discussion

For interpretation of the absorption profile of carbon monoxide on the microsecond and millisecond time scale inside the silica mesopores, previous static IR studies of CO adsorbed onto mesoporous and microporous silica sieves at low temperature are a valuable guide. Specifically, a study of the IR spectrum of CO adsorbed onto MCM-41 at 123 K by Tori et al.[23] suggests that the unusually broad, heterogeneous band profile over the first few hundred microseconds (Figures 3a and 4) originates from interaction of CO with various pore surface sites as the molecule escapes into the gas phase. The mesopore surface of

MCM-41 after calcination treatment under conditions used in this work possesses between one and two silanol groups per nm^2.[24] With a mesopore wall area of approximately 5500 nm^2 for a pore of 1 μ length, this density corresponds to approximately 5000 to 10 000 SiOH groups per mesopore. Carbon monoxide can interact with these SiOH groups either through C or O. The CO absorption upon Si−OH···CO interaction is shifted to the blue relative to free CO (2143 cm^{-1}), with the exact frequency depending on the microenvironment of the silanol group: 2160 cm^{-1} for the terminal silanol OH of clusters of H-bonded silanols, 2156 cm^{-1} for geminal silanols, and 2152 cm^{-1} for single SiOH groups.[23] This trend reflects the relative acidity of the OH groups, with the more acidic OH sites exhibiting the larger blue shift. CO molecules interacting with SiOH through the O end are red shifted and have been detected in low-temperature adsorption experiments at 2122 cm^{-1} (silicalite) and 2131 cm^{-1} (Aerosil).[25] A weak band has also been observed at 2108 cm^{-1} for CO in MCM-41 pores at 123 K,[23] which may be due to SiOH···OC species. At low temperature, the SiOH···OC configuration shows much lower absorbance than the SiOH···CO site. It has been demonstrated that the two configurations are at equilibrium and that the O-interacting form is less stable than SiOH···CO by about 2 kJ mol^{-1}.[25] Therefore, at room temperature, the equilibrium ratio of the SiOH···OC and SiOH···CO forms is predicted to be around 0.4. Since the extinction coefficient of the O-bonded form is estimated to be 2−3 times larger than that for the C-bonded form,[26] the absorptions of the two forms at room temperature are expected to be about equally intense. This is in good agreement with the two residual bands observed on the millisecond time scale in both plain and TMS-MCM-41, and we assign the two bands to these two species. Specifically, the blue-shifted band is assigned to SiOH···CO and the red-shifted band to SiOH···OC. Furthermore, all low-temperature spectra show a band attributed to physisorbed carbon monoxide (interacting with siloxane oxygen) in the region 2140−2136 cm^{-1}.[23,25,27,28] Taken together, the results from static FTIR studies of CO adsorbed on microporous and mesoporous silicas at low temperature indicate absorption bands with maxima ranging from 2160 to 2100 cm^{-1}, which coincides with the width of the CO band observed here on the microsecond time scale. We conclude that the initial broad absorption profile originates from CO transiently interacting with SiOH groups and siloxane oxygen as the molecules escape from the pores into the gas phase.

The observed kinetics of the fast-decaying CO profile further underpins the interpretation of the initial decay as CO diffusing by random hops out of the mesopores while interacting weakly with the wall. From the decay time, we estimate the macroscopic CO diffusion coefficient along the mesopores using the Einstein relation for a one-dimensional (1D) random walk[32]

$$D = \frac{\langle z^2(t)\rangle}{2t}$$

It is assumed that within the decay time $t = t_e$ (1/e time) as calculated from the exponential fit, the mean-square displacement of CO is equal to one pore length, that is, $\langle z^2(t_e)\rangle^{1/2} = 1$ μ. For plain MCM-41, we obtain $D = 1.5 \times 10^{-9}$ m^2/s (t_e = 344 μs), and for TMS−MCM-41, $D = 3.4 \times 10^{-9}$ m^2/s (t_e = 147 μs). While no diffusion coefficients have been reported for CO in MCM-41 or other mesoporous silicas, the constant for CO in silicalite (crystalline silica with MFI structure, 0.55 nm diameter pores in a 3D network)[33] has been reported as $D = 1.0 \times 10^{-8}$ m^2/s (295 K) using the PFG-NMR technique.[3] In zeolite theta-1 (crystalline silica with 0.46 nm diameter pores in a 1D network),[34] $D = 6.2 \times 10^{-10}$ m^2/s (295 K) has been measured using the frequency response technique.[7] Despite different pore structures and diameters, these silica materials give CO diffusion coefficients that lie within an order of magnitude of the coefficients determined here for mesoporous MCM-41 silica. This supports the notion that the fast CO component in MCM-41 is due to CO molecules interacting very weakly with the silanol and siloxane groups while diffusing through the mesopores.

It is important to note that the estimated diffusion coefficient of 1.5×10^{-9} m^2/s (plain MCM-41) is based on the assumption that the CO molecules are released from the pressed pellet after escape from the mesopores of the silica particle in which they were formed. According to the SEM image of a pressed wafer, the spaces between the MCM-41 particles form a loose, open network of micrometer-size macrovoids. The diffusion coefficient for hopping through the interparticle macrovoid network (assuming diameter of 1 μ, gas pressure below 10 mTorr) is estimated as $D_{inter} = 1 \times 10^{-4}$ m^2/s.[6] For a 100 μ thick pellet, random walk would give an escape time on the order of 10 μs; hence, the release from the pellet is expected to be short compared to the residence time of CO in the mesopores. While we consider the transport of CO to be controlled by intra MCM-41 particle diffusion rather than macrovoid diffusion (long-range diffusion),[35] we cannot rule out occasional re-entry of a CO molecule into the mesopores of another silica particle before eventual escape from the pellet. However, this process is not likely to play a major role because of the very weak interaction between CO and the silica pore surface[25] and the fact that only one-third of the particle surface features channel openings. Moreover, multiple re-entries would imply a mesopore diffusion constant for CO far above the range of values expected from the results of microporous silicas.[3,7]

A pronounced effect of trimethylsilylation of the pore surface is the much sharper absorption profile of the decreasing CO at early times, with a peak at 2137.5 cm^{-1} (Figure 7). This observation agrees with the expectation that the most readily escaping CO molecules (t_e = 147 μs) are the ones that are in contact with trimethylsilyl groups through weak van der Waals interactions. However, only about 15% of the CO escapes on the microsecond time scale; it takes 20 ms (Figure 8, inset) to release 60% of CO from trimethylsilylated MCM-41 as opposed to 500 μs for plain MCM-41. We attribute this to a large fraction of the photoexpelled CO getting initially entangled in the trimethylsilyl layer.

It is known from detailed studies of CO interacting with SiOH and Bronsted acid sites (Si−O^+(H)−Al) of zeolites of type Y (faujasite) and ZSM-5 (pentasil) that the blue shift of C-bonded and red shift of O-bonded CO increase with increasing acidity of the hydroxyl group. For example, Bronsted OH···CO and OH···OC absorptions for zeolite HY are at 2173 and 2124 cm^{-1}, respectively,[29,30] while for the more acidic acid sites in zeolite ZSM-5, the SiOH···OC band shifts to 2115 cm^{-1}.[26] Our observation that the SiOH···CO and SiOH···OC sites with the largest frequency shifts (2167 and 2105 cm^{-1} for plain MCM-41, 2175 and 2106 cm^{-1} for TMS-MCM-41) survive longer agrees with the expectation that the most strongly interacting sites persist the longest. Hence, we attribute these long-lived bands with residual CO more strongly held at SiOH groups. However, it does not explain why these CO molecules are released on a time scale that is 3 orders of magnitude slower compared to the initially released CO.

An important clue for understanding the unexpected slow escape of the residual CO absorbing at 2167 and 2105 cm^{-1} is the fact that these sites are populated immediately following photoelimination of CO from the precursor. Inspection of the CO decay profile in plain MCM-41 (Figure 3a and 4) and TMS-MCM-41 (Figure 7) shows that there is no growth of these peaks on the micro- or early millisecond time scale. In particular, no isosbestic point is observed. This implies that CO molecules hopping through the pores are not trapped at these sites. The only explanation we can conceive of for these long-lived sites is CO interacting with both surface SiOH and phenyl moieties of diphenyl acetylene coproduct: $SiOH\cdots CO\cdots C_6H_5CCC_6H_5$ absorbing at 2167 (2175) cm^{-1}, and $SiOH\cdots OC\cdots C_6H_5CCC_6H_5$ with a peak at 2105 (2106) cm^{-1}, or possibly even those of additional precursor molecules nearby. That is, we believe that these CO molecules are trapped by the coproduct and/or precursor molecules on the pore surface. While the spectral observations do not allow us to determine details of the interaction of CO with surrounding hydrocarbon molecules, the data clearly show that these sites are only formed by DPCP photodissociation and are not populated by random hopping CO molecules. The observed kinetics reflects the rate-limiting escape from the cluster, which is followed by the much faster diffusion through the pores on the sub-millisecond time scale. We conclude that the residual, long-lived species are a consequence of the particular choice of the precursor. Indeed, the corresponding bands are not observed when using an alternate precursor like cyclohexanone.[36] However, for the study of CO diffusion in mesopores at RT unencumbered by mobile precursor molecules, which is the goal of the work reported here, use of a nonvolatile photolabile CO source like DPCP is required.

5. Conclusions

This study is the first to provide spectroscopic data on the sites occupied by CO and on the diffusion kinetics in a mesoporous material at room temperature. The measurements in plain MCM-41 reveal biphasic kinetics, with the fast, major component (microsecond) associated with the escape of CO physisorbed on the pore surface or weakly interacting with surface silanol groups and the residual slow component (millisecond) originating from molecules trapped between silanol OH groups and diphenyl acetylene coproduct and, possibly, precursor molecules. The time-resolved FTIR data afford a view of the behavior of CO inside silica mesopores at ambient temperature that is unprecedented in its detail. This knowledge will be particularly useful for the mechanistic understanding of CO_2 photoreduction in nanoporous transition metal silica hosts. The finding that CO escapes from the mesopores at room temperature in less than a millisecond shows that the nanoporous silica environment will not limit photocatalytic turnover rates and is favorable in terms of preventing back reaction.[2]

Acknowledgment. This work was supported by the Director, Office of Science, Office of Basic Energy Sciences, Division of Chemical, Geological and Biosciences of the U.S. Department of Energy under Contract No. DE-AC03-76SF00098. The authors thank Mr. Michael Grass (Somorjai group) for conducting pore size distribution measurements.

References and Notes

(1) Lin, W.; Frei, H. *J. Am. Chem. Soc.* **2005**, *127*, 1610.
(2) Lin, W.; Han, H.; Frei, H. *J. Phys. Chem. B* **2004**, *108*, 18269.
(3) Karger, J.; Pfeifer, H.; Stallmach, F.; Feoktistova, N. N.; Zhdanov, S. P. *Zeolites* **1993**, *13*, 50.
(4) Stallmach, F.; Karger, J.; Pfeifer, H. *J. Magn. Reson., Ser. A* **1993**, *102*, 270.
(5) Rittig, F.; Coe, C. G.; Zielinski, J. M. *J. Am. Chem. Soc.* **2002**, *124*, 5264.
(6) Rittig, F.; Coe, C. G.; Zielinski, J. M. *J. Phys. Chem. B* **2003**, *107*, 4560.
(7) Shen, D.; Rees, L. V. C. *J. Chem. Soc., Faraday Trans.* **1994**, *90*, 3017.
(8) Rittig, F.; Farris, T. S.; Zielinski, J. M. *AIChE J.* **2004,** *50*, 589.
(9) Aksnes, D. W.; Forland, K.; Stocker, M. *Microporous Mesoporous Mater.* **2005**, *77*, 79.
(10) Stallmach, F.; Graser, A.; Karger, J.; Krause, C.; Jeschke, M.; Oberhagemann, U.; Spange, S. *Microporous Mesoporous Mater*. **2001**, *44*, 745.
(11) Courivaud, F.; Hansen, E. W.; Karlsson, A.; Klaboe, S.; Stocker, M. *Microporous Mesoporous Mater*. **2000**, *35*, 327.
(12) Yeom, Y. H.; Frei, H. In *In-situ Characterization of Catalysts*; Weckhuysen, B. M., Ed.; American Scientific Publisher: 2004; p 32.
(13) Yeom, Y. H.; Frei, H. *J. Phys. Chem. B* **2003**, *107*, 6286.
(14) Vasenkov, S.; Frei, H. *J. Phys. Chem. A* **2000**, *104*, 4327.
(15) Vasenkov, S.; Frei, H. In *Molecular and Supermolecular Photochemistry*; Ramamurthy, V., Schanze, K. S., Eds.; Marcel Dekker: New York, 2000; Vol. 5, p 295.
(16) Vasenkov, S.; Frei, H. *J. Am. Chem. Soc.* **1998**, *120*, 4031.
(17) Takeuchi, S.; Tahara, T. *J. Chem. Phys.* **2004**, *12*, 4768.
(18) Lin, W.; Cai, Q.; Pang, W.; Yue, Y.; Zou, B. *Microporous Mesoporous Mater*. **1999**, *33*, 187.
(19) Sever, R. R.; Alcala, R.; Dumesic, J. A.; Root, T. W. *Microporous Mesoporous Mater*. **2003**, *66*, 53.
(20) Beck, J. S.; Vartuli, J. C.; Roth, W. J.; Leonowicz, M. E.: Kresge, C. T.; Schmitt, K. D.; Chu, C. T. W.; Olsen, D. H.; Sheppard, E. W.; McCullen, S. B.; Higgins, J. B.; Schlenker, J. L. *J. Am. Chem. Soc.* **1992**, *114*, 10834.
(21) Broyer, M.; Valange, S.; Bellat, J. P.; Bertrand, O.; Weber, G.; Gabelica, Z. *Langmuir* **2002,** *18*. 5083.
(22) Blatter, F.; Frei, H. *J. Am. Chem. Soc.* **1994**, *116*, 1812.
(23) Mori, T.; Kuroda, Y.; Yoshikawa, Y.; Nagao, M.; Kittaka, S. *Langmuir* **2002**, *18*, 1595.
(24) Zhao, X. S.; Lu, G. Q.; Whittaker, A. K.; Millar, G. J.; Zhu, H. Y. *J. Phys. Chem. B* **1997**, *101*, 6525.
(25) Storozhev, P. Y.; Arean, C. O.; Garrone, E.; Ugliengo, P.; Ermoshin, V. A.; Tsyganenko, A. A. *Chem. Phys. Lett*. **2003**, *374*, 439.
(26) Ugliengo, P.; Garrone, E.; Ferrari, A. M.; Zecchina, A.; Arean, C. O. *J. Phys. Chem. B* **1999**, *103*, 4839.
(27) Zecchina, A.; Scarano, D.; Spoto, G.; Bordiga, S.; Lamberti, C.; Bellussi, G. *Stud. Surf. Sci. Catal*. **1998**, *117*, 343.
(28) Zecchina, A.; Bordiga, S.; Spoto, G.; Marchese, L.; Petrini, G.; Leofanti, G.; Padovan, M. *J. Phys. Chem*. **1992**, *96*, 4991.
(29) Arean, C. O.; Tsyganenko, A. A.; Manoilova, O. V.; Palomino, G. T.; Mentruit, M. P.; Garrone, E. *Chem. Commun.* **2001**, 455.
(30) Arean, C. O.; Manoilova, O. V.; Tsyganenko, A. A.; Palomino, G. T.; Mentruit, M. P.; Geobaldo, F.; Garrone, E. *Eur. J. Inorg. Chem*. **2001**, 1739.
(31) Smith, A. L. *The Coblentz Society Desk Book of Infrared Spectra;* Carver, C. D., Ed.; The Coblentz Society: Kirkwood, MO, 1982.
(32) Karger, J.; Ruthven, D. M. *Diffusion in Zeolites and Other Microporous Solids*; Wiley: New York, 1992; p 5.
(33) Meier, W. M.; Olson, D. H.; Baerlocher, C. *Atlas of Zeolite Structure Types*; Elsevier: London, 1996; p 146.
(34) Meier, W. M.; Olson, D. H.; Baerlocher, C. *Atlas of Zeolite Structure Types*; Elsevier: London, 1996; p 194.
(35) Karger, J.; Vasenkov, S. *Microporous Mesoporous Mater*. **2005**, *85*, 195.
(36) Andersen, L.; Frei, H., to be submitted for publication.